

## Conference paper

Prabhat Ranjan\*, Praveen K. Surolia and Tanmoy Chakraborty\*

# Structure, electronic and optical properties of chalcopyrite-type nano-clusters $XFeY_2$ ( $X=Cu, Ag, Au$ ; $Y=S, Se, Te$ ): a density functional theory study

<https://doi.org/10.1515/pac-2020-1202>

**Abstract:** Iron-based chalcopyrite materials have diverse applications in solar cells, spintronic, thermoelectric devices, LEDs and medical sciences. In this report we have studied structure, electronic and optical properties of chalcopyrite-type nano-cluster  $XFeY_2$  ( $X=Cu, Ag, Au$ ;  $Y=S, Se, Te$ ) systematically by using Density Functional Theory (DFT). Our computed HOMO-LUMO energy gap of  $XFeY_2$  is in the range of 1.568–3.982 eV, which endorses its potential application in optoelectronic devices and solar cells. The result shows that chalcopyrite-type material  $AuFeS_2$  having a star-type structure with point group  $C_{2v}$  and sextet spin multiplicity, is the most stable cluster with HOMO-LUMO energy gap of 3.982 eV. The optical properties viz. optical electronegativity, refractive index, dielectric constant, IR and Raman activity of these nano-clusters are also investigated. The result exhibits that HOMO-LUMO energy gap of  $XFeY_2$  along with optical electronegativity and vibrational frequency decreases from S to Se to Te, whereas refractive index and dielectric constant increases in the reverse order.

**Keywords:**  $AuFeS_2$ ; chalcopyrite-type nano-cluster; chemistry and its applications; DFT; HOMO-LUMO energy gap; solar cells; VCCA-2020.

## Introduction

Transition-metals based chalcopyrites are significant type of earth materials which display various electronic, optical, magnetic and catalytic properties [1, 2]. Ternary semiconducting materials I-III-VI<sub>2</sub> are considered as the most promising candidate for thin-film sensitizers due to their distinctive physico-chemical properties like high values of absorption coefficients and conversion efficiency, tunable band gap and less toxicity [3–10]. Fe-based chalcopyrites are promising materials from industrial as well as technological point of view. It is well established through a number of reports that these materials provide very important and diverse physico-chemical properties [11–18]. It has a wide range of technological applications in solar cells, spintronics, optical devices, sensing devices, LEDs, thermoelectric devices *etc.* [11–18].

Chalcopyrite materials  $CuFeS_2$  and  $AgFeS_2$  are part of novel ternary semiconductor family I-III-VI<sub>2</sub> with band gap of 0.5 and 0.9 eV respectively [3, 19–21]. Dutkova *et al.* [19] reported the optical band gap of  $CuFeS_2$  nanoparticles as 1.05 eV which is high as compared to the bulk chalcopyrite. Study reveals that bulk

---

**Article note:** A collection of invited papers based on presentations at the Virtual Conference on Chemistry and its Applications (VCCA-2020) held on-line, 1–31 August 2020.

---

**\*Corresponding authors:** Prabhat Ranjan, Department of Mechatronics Engineering, Manipal University Jaipur, Dehmi-Kalan, Jaipur 303007, India, e-mail: prabhat23887@gmail.com; and Tanmoy Chakraborty, Department of Chemistry and Biochemistry, School of Basic Sciences and Research, Sharda University, Greater Noida 201310, India, e-mail: tanmoychem@gmail.com  
Praveen K. Surolia, Department of Chemistry, Manipal University Jaipur, Dehmi-Kalan, Jaipur 303007, India

chalcopyrite  $CuFeS_2$  shows semiconducting and magnetic nature with low optical band gap of 0.5 eV, however at nano-scale it displays a high band gap with unique electronic, optical and magnetic properties [20]. Conejeros *et al.* [2] investigated the electronic structure and magnetic behaviour of  $CuFeS_2$ . They proved that chalcopyrite material  $CuFeS_2$  displays an antiferromagnetic behaviour at the ground state. Takaki *et al.* [22] investigated the Seebeck coefficient in magnetic semiconducting material  $CuFeS_2$  and found that Seebeck coefficient is governed by its electronic structure. Zhou *et al.* [23] studied the semiconducting and magnetic nature of  $CuFeS_2$  by using Density Functional Theory (DFT) method. They found that it is a semiconducting material with band gap of 0.5 eV and magnetic moment of  $3.64 \mu_B$  per Fe atom.

Sciacca *et al.* [3] found that  $AgFeS_2$  chalcopyrite covers the complete visible spectrum and shows a large absorption coefficient. Recently, Djaafri *et al.* [24] reported by using DFT technique that chalcopyrite material  $AgFeS_2$  displays equivalent magnetic sequence as  $CuFeS_2$ . They also stated that it shows semiconducting properties with an indirect band gap. Peng *et al.* [25] studied nanoparticles of  $AgFeS_2$  and its applications in artery stenosis therapy by using DFT technique. For the localized 3d electron of iron atoms authors have found large absorption spectra over wide-band region which is in line with the UV-Vis-NIR spectrum.

The importance of relativistic effects especially for heavy compounds is well established by the researchers [26]. It has significant role in study of their geometry as well as physical and chemical properties [27–29]. Study shows that relativistic effect is vital to understand the structural chemistry and electronic state for heavy elements [30]. Relativistic configuration interaction calculations are reported for molecular system  $SnO^+$ ,  $PbO^+$ ,  $PbS^+$  and  $PbSe^+$  [31]. Balasubramanian *et al.* [32] investigated the relativistic effect for compound  $TeH$ . Authors reported that in the case of  $TeH$  system spin-orbit splitting and contamination is more due to its open shell ground state. Balasubramanian *et al.* [33] studied the spectroscopic properties of system  $Te_2$ . They found that spin-orbit arrangement plays important role in understanding the electronic states of  $Te_2$  system.

In this report, we have investigated the structure, optical and electronic properties of chalcopyrite-type nano-cluster  $XFeY_2$  ( $X=Cu, Ag, Au$ ;  $Y=S, Se, Te$ ) by using DFT technique. The ground state configuration and low-lying isomers of each cluster have no imaginary vibrational frequencies. The DFT based global descriptors- Highest Occupied Molecular Orbital (HOMO)- Lowest Unoccupied Molecular Orbital (LUMO) gap, molecular hardness, softness, electronegativity, electrophilicity index and dipole moment of these nano-clusters are studied. The optical electronegativity, refractive index, dielectric constant and IR and Raman activity of chalcopyrite-type nano-cluster  $XFeY_2$  are also computed.

## Methodology

DFT is a very successful technique among several computational methods used for electronic structure calculation. It has opened many new dimensions in material sciences, physics, chemistry, surface science, nanotechnology, biology and earth sciences [34–38]. DFT has gained significant importance in aromaticity, electronic stability and dynamics of molecular system [39–46]. In this report, computational study on the chalcopyrite-type nano-clusters of  $XFeY_2$  ( $X=Cu, Ag, Au$ ;  $Y=S, Se, Te$ ) is performed within Density Functional Theory (DFT) framework. Modelling and geometry optimizations of nano-clusters are done by using computational software Gaussian 03 [47]. The Generalized Gradient Approximation (GGA) B3PW91 with basis set LanL2dz is implemented for geometry optimization. GGA functional is popular for computation of chalcopyrite-type semiconducting materials [48–53]. Recent work on chalcopyrite-type materials by using B3PW91/LanL2dz encourages to choose this functional for  $XFeY_2$  [54, 55].

With the help of Koopman's approximation [56], Ionization Potential ( $I$ ) and Electron Affinity ( $A$ ) of  $XFeY_2$  nano-clusters are computed through the following approach:

$$I = -\epsilon_{HOMO} \quad (1)$$

$$A = -\epsilon_{LUMO} \quad (2)$$

Subsequently, by using  $I$  and  $A$ , the conceptual DFT based descriptors viz. Highest Occupied Molecular orbital (HOMO) – Lowest Unoccupied Molecular Orbital (LUMO) energy gap, electronegativity ( $\chi$ ), molecular hardness ( $\eta$ ), softness ( $S$ ) and electrophilicity index ( $\omega$ ) are calculated as under:

$$\chi = -\mu = \frac{I + A}{2} \quad (3)$$

where,  $\mu$  represents the chemical potential of the system.

$$\eta = \frac{I - A}{2} \quad (4)$$

$$S = \frac{1}{2\eta} \quad (5)$$

$$\omega = \frac{\mu^2}{2\eta} \quad (6)$$

The optical electronegativity is an important parameter to investigate the chemical bonding and other physical and chemical properties of chalcopyrite-type materials [57]. In order to establish a relationship among optical electronegativity and energy gap, Duffy [58, 59] introduced the following approach:

$$\Delta\chi^* = 0.2688E_g \quad (7)$$

where,  $\Delta\chi^* = \chi_{anion}^* - \chi_{cation}^*$ ,  $\chi^*$  are the optical electronegativities of anion and cation respectively.

Refractive index is a vital factor to compute the optical properties of chalcopyrite-type materials. Moss [60–62] introduced firstly the relationship among refractive index and band gap of materials, which is as follow:

$$n^4 E_g = 95 \text{ eV} \quad (8)$$

where  $n$  and  $E_g$  are refractive index and band gap of semiconducting materials respectively. By using Eqs. (7) and (8), Moss relation in terms of optical electronegativity and refractive index can be written as:

$$n = \frac{2.247}{(\Delta\chi^*)^{1/4}} \quad (9)$$

Ravindra and his team [63, 64] worked extensively on the refractive index of chalcopyrite-type semiconductors. The relationship between refractive index and band gap established by them is as follow:

$$n = 4.084 - 0.62E_g \quad (10)$$

Ravindra's equation provides the good results for materials with small and medium energy gap. With the help of Eqs. (7) and (10), Ravindra's equation can be written in terms of optical electronegativity as:

$$n = 4.084 - 2.306\Delta\chi^* \quad (11)$$

Herve *et al.* [65, 66] established the following relationship between refractive index and band gap. It is suitable for materials with band gap higher than 1.4 eV.

$$n = \sqrt{1 + \left(\frac{A}{E_g + B}\right)^2} \quad (12)$$

where  $A$  is the ionization energy of hydrogen and  $B$  is constant (variation in the UV resonance energy and band gap). The values of  $A$  and  $B$  are 13.6 and 3.47 eV respectively. In terms of optical electronegativity, this equation can be written as:

$$n = \sqrt{1 + \left( \frac{A}{3.72\Delta\chi^* + B} \right)^2} \quad (13)$$

Reddy and his group [57, 67] introduced the relationship between refractive index and band gap as:

$$n = \left( \frac{154}{E_g - 0.365} \right)^{1/4} \quad (14)$$

In terms of optical electronegativity, Eq. (14) can be written as:

$$n = \left( \frac{154}{3.72\Delta\chi^* - 0.365} \right)^{1/4} \quad (15)$$

In this report, refractive index of chalcopyrite-type nano-clusters  $XFeY_2$  are computed by using Eqs. (9), (11), (13) and (15).

The dielectric constant of semiconducting materials plays important role in designing of the electronic devices. It helps in understanding the function of charge carriers, dopants, defects and impurities of insulators and semiconductors [68]. Lorentz-Lorenz established that dielectric constant is equal to square of refractive index of semiconducting materials, which is as follow:

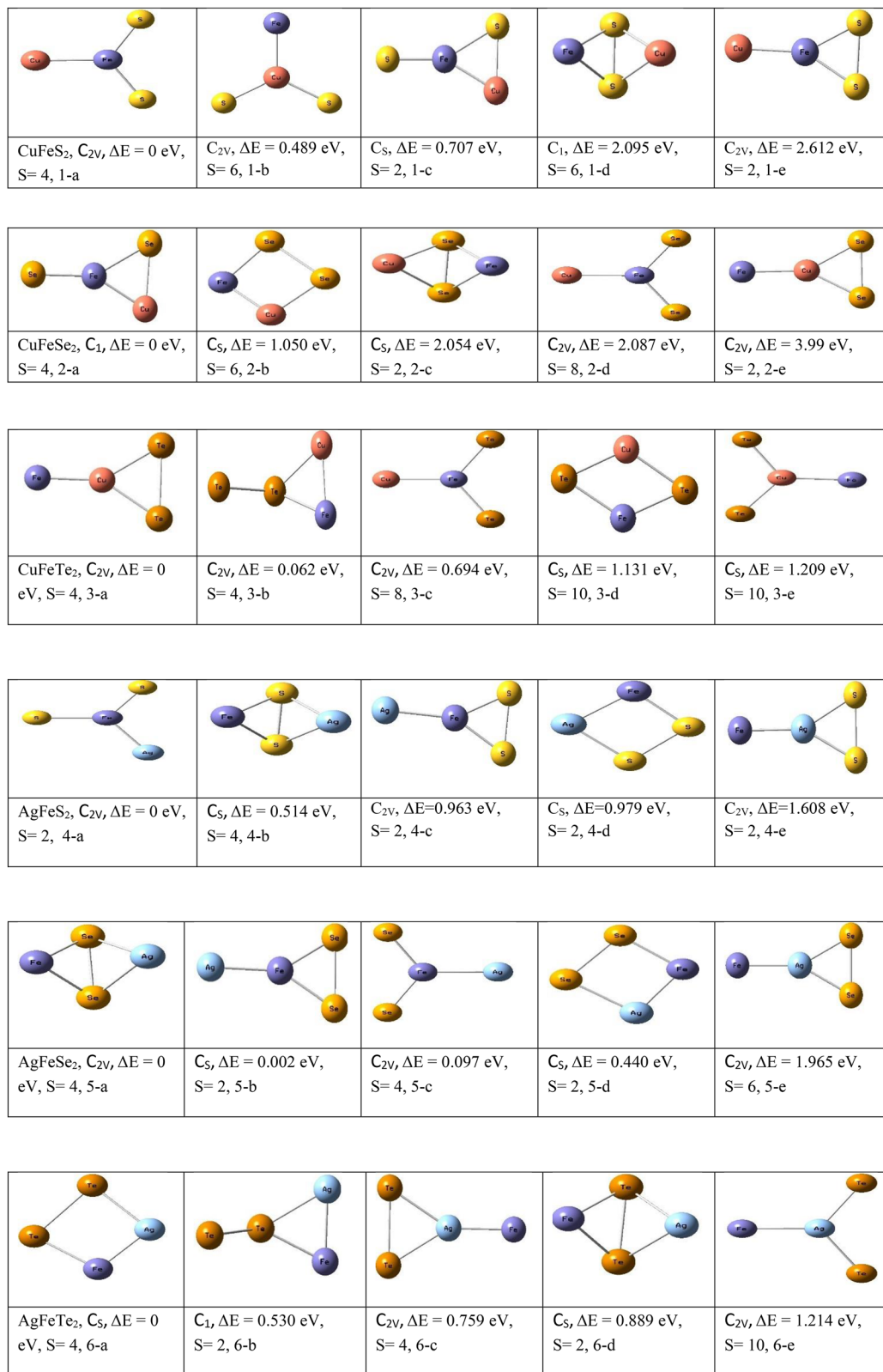
$$\epsilon = n^2 \quad (16)$$

## Results and discussion

### Equilibrium geometries

The ground state configuration and low lying isomers of chalcopyrite-type nano-cluster  $XFeY_2$  ( $X=Cu, Ag, Au$ ;  $Y=S, Se, Te$ ) are studied and presented in Figure 1. We have optimized various geometries during the search for the most stable structure; however, five lowest energy structures are presented in Figure 1 for each cluster. For  $CuFeS_2$  cluster, the most stable structure and its isomers are optimized in the energy range of 0–2.65 eV. The ground state configuration (1-a) with point group  $C_{2V}$  and quartet spin multiplicity is a star-type structure in which Fe atom is placed at the centre and all other atoms are directly connected from it. The isomer 1-b with symmetry group  $C_{2V}$  and spin multiplicity sextet is obtained from structure 1-a by exchanging the position of Fe and Cu atoms. However, isomer 1-b is energetically less stable than 1-a by 0.489 eV. Isomer 1-c with point group  $C_S$  and doublet spin is less stable than structures 1-a and 1-b by 0.707 and 0.218 eV respectively. Isomer 1-d with point group  $C_1$  and sextet spin state is a rectangular structure in which sulphur atoms are placed at opposite end. It is 2.095 eV higher in energy as compared to the most stable structure 1-a. Isomer 1-e with symmetry group  $C_{2V}$  and spin multiplicity doublet is derived from 1-c by swapping Cu and S atoms. Energetically isomer 1-e is less stable than 1-a and 1-d by 2.612 and 0.517 eV respectively.

For nano-cluster  $CuFeSe_2$ , ground state configuration and low lying isomers are optimized in the energy range of 0–4.0 eV. The most stable structure (2-a) with symmetry group  $C_1$  and quartet spin multiplicity is having Fe atom at the centre and forms a triangular geometry with Cu and Se atoms. The isomer 2-b with point group  $C_S$  and spin multiplicity sextet is a rectangular structure with 1.050 eV less stable than the most stable isomer 2-a. The isomer 2-c with symmetry group  $C_S$  and spin multiplicity doublet is optimized from 2-b by swapping Cu and Se atoms. It is of high energy than isomers 2-a and 2-b by 2.054 and 1.004 eV respectively. Isomer 2-d with point group  $C_{2V}$  and spin multiplicity octet is a star-type structure. It is 2.087 eV energetically less stable than the most stable structure 2-a. However, the energy difference among isomers 2-c and 2-d is only 0.033 eV. Isomer 2-e with point group  $C_{2V}$  and spin state doublet is 3.99 eV less stable than the lowest energy structure 2-a.


**Figure 1:** The ground state configurations of  $XFeY_2$  ( $X=Cu, Ag, Au$  and  $Y=S, Se, Te$ ) chalcopyrite-type nano-cluster.

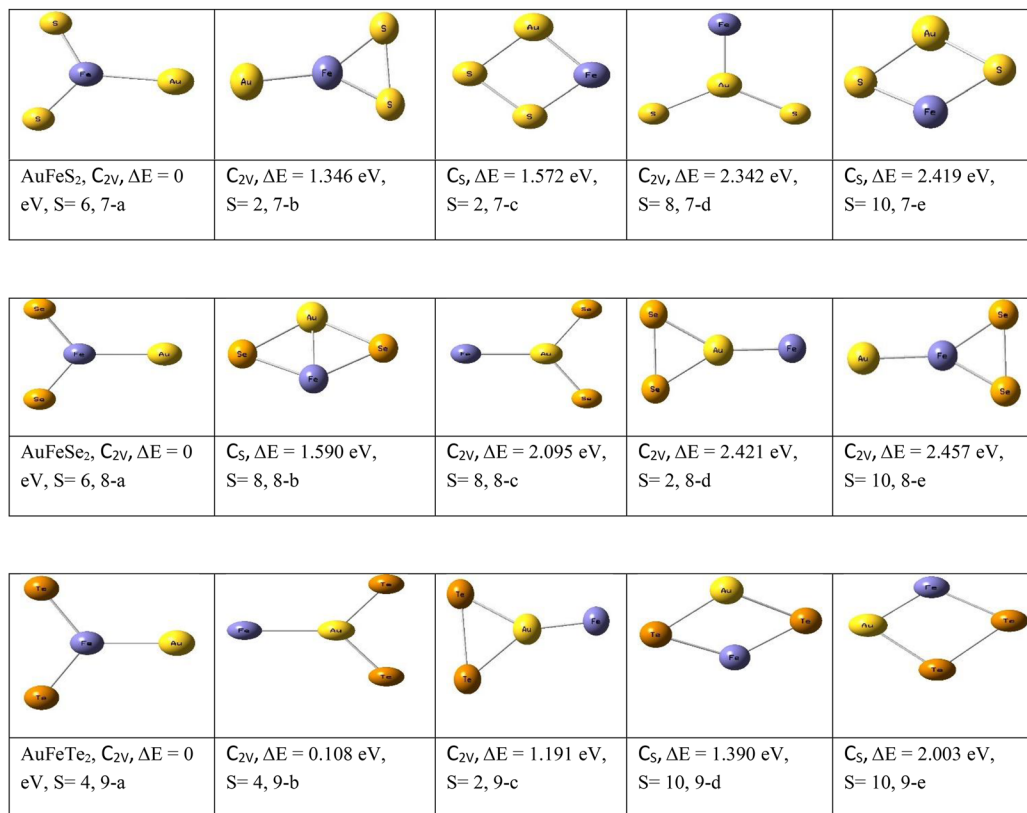


Figure 1: Continued.

The most stable isomer of  $CuFeTe_2$  (3-a) with symmetry group  $C_{2v}$  and quartet spin multiplicity forms a triangular structure with Cu and Te atoms. Isomer 3-b with point group  $C_{2v}$  and spin state quartet is designed from the most stable structure 3-a by exchanging the position of atoms. It has Te atom at the centre and forms a triangular structure with Fe and Cu atoms. Isomer 3-b is less stable than 3-a by 0.062 eV. Isomer 3-c with point group  $C_{2v}$  and spin multiplicity octet is a star-type structure with Fe atom at the centre. Energetically isomer 3-c is less stable than 3-a and 3-b by 0.694 and 0.632 eV respectively. Isomer 3-d is a rectangular structure with symmetry group  $C_s$  and spin multiplicity dectet. It is 1.131 eV less stable than the ground state configuration 3-a. Isomer 3-e with point group  $C_s$  and spin multiplicity dectet is a star-type structure obtained from 3-c by swapping the position of Cu and Fe atoms. It is energetically 1.209 eV less stable than the most stable isomer 3-a. However, it is only 0.078 eV higher in energy than 3-d.

For  $AgFeS_2$  nano-cluster, ground state configuration (4-a) is a star-type structure with symmetry group  $C_{2v}$  and spin multiplicity doublet. Isomer 4-b with symmetry group  $C_s$  and spin multiplicity quartet is a rectangular structure in which both sulphur atoms are placed at opposite end. It is 0.514 eV less stable than the lowest energy structure 4-a. Isomer 4-c with symmetry group  $C_{2v}$  and spin doublet is less stable than 4-a and 4-b by 0.963 and 0.449 eV respectively. Isomer 4-d with symmetry group  $C_s$  and spin multiplicity doublet is obtained from 4-b. It is 0.979 eV less stable than structure 4-a. However, it is energetically close to isomer 4-c with energy difference of only 0.016 eV. Isomer 4-e with point group  $C_{2v}$  and spin multiplicity doublet is found from 4-c by exchanging the position of Ag and Fe atoms. It is 1.608 eV less stable than the ground state configuration 4-a.

The ground state configuration (5-a) of  $AgFeSe_2$  nano-cluster is a rectangular structure with point group  $C_{2v}$  and spin multiplicity quartet. It is observed that isomer 5-b with symmetry group  $C_s$  and spin multiplicity doublet is energetically very close to the most stable structure 5-a. Isomer 5-c with symmetry group  $C_{2v}$  and spin quartet is star-type structure, it is 0.097 eV less stable than the structure 5-a. Isomer 5-d is obtained from the

most stable structure 5-a by exchanging the position of Ag and Se atoms. It is less stable than the isomer 5-a by 0.440 eV. Isomer 5-e with point group  $C_{2V}$  and spin multiplicity sextet is found from 5-b by swapping Ag and Fe atoms. Energetically it is less stable than the most stable isomer 5-a by 1.965 eV.

The most stable structure (6-a) of  $AgFeTe_2$  nano-cluster is a rectangular-shape geometry with point group  $C_S$  and spin multiplicity quartet. Isomer 6-b with symmetry group  $C_1$  and spin multiplicity doublet is 0.530 eV less stable than the most stable structure. Isomer 6-c with point group  $C_{2V}$  and spin multiplicity quartet is less stable than isomers 6-a and 6-b by 0.759 and 0.229 eV respectively. Isomer 6-d with symmetry group  $C_S$  and spin multiplicity doublet is rectangular structure in which both Te atoms placed at opposite end. It is less stable by 0.889 eV than the most stable isomer 6-a. The energy difference between isomers 6-c and 6-d is 0.13 eV. Isomer 6-e with symmetry group  $C_{2V}$  and spin multiplicity dectet is a star-type structure in which Ag atom is at the centre. It is 1.214 eV less stable than the ground state configuration 6-a.

The ground state configuration (7-a) of  $AuFeS_2$  nano-cluster is a star-type structure with point group  $C_{2V}$  and spin multiplicity sextet in which Fe atom is placed at the centre. Isomer 7-b with symmetry group  $C_{2V}$  and spin doublet is less stable than the most stable isomer 7-a by 1.346 eV. Isomer 7-c with symmetry group  $C_S$  and spin multiplicity doublet is a rectangular structure with Ag and S atoms are placed on the opposite end. It is 1.572 eV less stable than the most stable isomer 7-a. The energy difference between isomers 7-b and 7-c is 0.226 eV. Isomer 7-d with symmetry group  $C_{2V}$  and spin multiplicity octet is a star-type structure in which Au atom is at the centre. It is 2.342 eV less stable than the ground state configuration 7-a. Isomer 7-e with symmetry group  $C_S$  and spin multiplicity dectet is obtained from structure 7-c by exchanging the position of Fe and S atoms. It is 2.419 eV less stable than the most stable isomer 7-a. However, the energy difference between isomers 7-d and 7-e is 0.077 eV.

The most stable isomer (8-a) of nano-cluster  $AuFeSe_2$  is a star-type structure in which Fe atom is placed at centre. It has symmetry group  $C_{2V}$  and spin multiplicity sextet. Isomer 8-b with symmetry group  $C_S$  and spin multiplicity octet is a rectangular structure in which Au and Fe are placed on the opposite end. It is 1.590 eV less stable than the ground state configuration 8-a. Isomer 8-c with symmetry group  $C_{2V}$  and spin multiplicity octet is 2.095 eV less stable than the isomer 8-a. However, the energy difference between isomers 8-b and 8-c is 0.505 eV. Isomer 8-d with symmetry group  $C_{2V}$  and doublet spin is 2.421 eV less stable than structure 8-a. However, isomer 8-d is 0.326 eV higher in energy than 8-c. Isomer 8-e with symmetry group  $C_{2V}$  and spin multiplicity dectet is less stable than the most stable structure 8-a by 2.457 eV. It is energetically close to isomer 8-d with energy difference of only 0.036 eV.

The ground state configuration (9-a) of  $AuFeTe_2$  is star-type geometry in which Fe atom at the centre. It has symmetry group  $C_{2V}$  and spin multiplicity quartet. Isomer 9-b with point group  $C_{2V}$  and spin multiplicity quartet is obtained from structure 9-a. It is less stable than isomer 8-a by 0.108 eV. Isomer 9-c with point group  $C_{2V}$  and spin multiplicity doublet is less stable by 1.1.91 eV than the most stable structure 9-a. Isomer 9-d with symmetry group  $C_S$  and spin multiplicity dectet is rectangular structure with both Te atoms lying at opposite end. It is 1.390 eV less stable than the most stable isomer 9-a. Isomer 9-e with symmetry group  $C_S$  and spin multiplicity dectet is obtained from structure 9-d by swapping Au and Te atoms. It is 2.003 eV less stable than the ground state configuration 9-a.

## Electronic properties and DFT based descriptors

The electronic properties and density functional theory based global descriptors of chalcopyrite-type nano-cluster  $XFeY_2$  ( $X=Cu, Ag, Au$ ;  $Y=S, Se, Te$ ) are studied in this section. The frontier orbitals, the Highest Occupied Molecular orbital (HOMO) and the Lowest Unoccupied Molecular Orbital (LUMO) play a significant role for donor-acceptor complexes [69]. It is established that HOMO and LUMO of both donor and acceptor are responsible for movement of charge and bonding during the evolution of donor-acceptor complexes [69]. The synchronous process of charge transfers to acceptor LUMO from donor HOMO and then to donor LUMO from acceptor HOMO reveals the establishment transpires in donor-acceptor system [69]. The energy difference between HOMO and LUMO is an important factor to study the electronic properties of chalcopyrite-type

semiconductors [55]. It specifies the minimum energy required for a charge carrier to move from occupied orbital to unoccupied orbital.

The density functional theory based global descriptors along with dipole moment of  $XFeY_2$  are presented in Table 1. The result specifies that HOMO-LUMO energy gap of  $CuFeY_2$  is in the range of 1.573–1.855 eV, the maximum energy gap is obtained for nano-cluster  $CuFeS_2$  whereas  $CuFeTe_2$  displays the least energy gap. The computed data for chalcopyrite material  $CuFeS_2$  is in agreement with the previous reported results [2, 70]. Conejeros *et al.* [2] reported the band gap of antiferromagnetic configuration of  $CuFeS_2$  is 1.82 eV. Bhattacharyya *et al.* [70] reported that energy gap of  $CuFeS_2$  is in the range of 0.5–2 eV (600–2500 nm). Dutkova *et al.* [19] reported the band gap of  $CuFeSe_2$  nanoparticles is 0.95 eV. For  $AgFeY_2$ , energy gap varies between 1.576 and 2.703 eV. Maximum HOMO-LUMO energy gap is found for  $AgFeS_2$  whereas  $AgFeTe_2$  shows the minimum gap. Experimentally it is reported that band gap of nanocrystal  $AgFeS_2$  is in the range of 0.88–1.2 eV [3, 71]. The computed energy gap for  $AgFeX_2$  is in well agreement with the reported theoretical results [24, 72]. For chalcopyrite nano-cluster  $AuFeY_2$ , energy gap is in the range of 1.568–3.982 eV. The maximum HOMO-LUMO gap is observed for  $AuFeS_2$  whereas  $AuFeTe_2$  displays the least gap. The computed energy gap of  $XFeY_2$  is in the range of 1.568–3.982 eV, which indicates their potential applications in photovoltaics, optoelectronic devices and medical sciences [19, 24, 25, 55, 73]. The result reveals that energy gap for nano-cluster  $XFeY_2$  decreases from S to Se to Te, which is in line with the experimental and theoretical results reported for chalcopyrite-type semiconducting materials [57, 74–76]. Study shows that the relativistic effects on the electronic properties of heavy compounds help to reduce the considerable energy gap. For system containing S, Se and Te energy gap reduces due to the relativistic contraction of the s level. In the case of Te, relativistic effects decrease subsequently the s-p energy gaps of heavier elements [30]. For  $XFeY_2$  ( $X=Cu, Ag, Au; Y=S, Se, Te$ ) nano-clusters, HOMO-LUMO energy gap follow the order as  $Cu < Ag < Au$ .

The electronegativity concept is a key parameter for realization the charge transfers among donor and acceptor [77–82]. The computed electronegativity of nano-cluster  $XFeY_2$  are in the range of 4.117–5.660 eV. The maximum value of electronegativity is found for cluster  $AgFeTe_2$  whereas the minimum value is observed for cluster  $AgFeSe_2$ .

Pearson in his novel work stated that “every molecule tries to assemble themselves as hard as possible” [83]. Molecular hardness is a significant parameter to understand the molecular structure, stability, binding and dynamics of chemical species [84]. It is reported that molecular hardness of species increases when it moves from an unsteady state to steady state whereas when it moves from steady state to unsteady state, value of molecular hardness decreases [69]. The computed result shows that molecular hardness of  $XFeY_2$  have a direct relationship with HOMO-LUMO energy gap. Maximum hardness value is observed for nano-cluster  $AuFeS_2$  whereas  $AuFeTe_2$  displays the least value. It specifies that for molecular system  $XFeY_2$ ,  $AuFeS_2$  is the most stable cluster.

**Table 1:** Computed DFT based descriptors of  $XFeY_2$  ( $X=Cu, Ag, Au; Y=S, Se, Te$ ) chalcopyrite-type nano-cluster.

Species	HOMO-LUMO gap (eV)	Electronegativity (eV)	Hardness (eV)	Softness (eV)	Electrophilicity index (eV)	Dipole moment (Debye)
$CuFeS_2$	1.855	5.535	0.927	0.539	16.516	0.336
$CuFeSe_2$	1.788	5.478	0.894	0.559	16.787	4.330
$CuFeTe_2$	1.573	4.573	0.786	0.636	13.299	6.727
$AgFeS_2$	2.703	4.354	1.351	0.370	7.015	5.041
$AgFeSe_2$	2.457	4.117	1.228	0.407	6.899	3.286
$AgFeTe_2$	1.576	5.660	0.788	0.635	20.331	1.858
$AuFeS_2$	3.982	5.233	1.991	0.251	6.876	1.900
$AuFeSe_2$	3.718	5.157	1.859	0.269	7.152	1.224
$AuFeTe_2$	1.568	5.574	0.784	0.638	19.819	1.204

The molecular softness of chalcopyrite-type nano-cluster  $XFeY_2$  is computed and presented in Table 1. Molecular softness of these clusters is in the range of 0.251–0.638 eV. Minimum value of softness is observed for  $AuFeS_2$  whereas  $AuFeTe_2$  displays the maximum value. Cluster with maximum HOMO-LUMO energy gap shows the minimum softness values and vice-versa.

The electrophilicity index is a factor to check how much energy is being reduced because of excessive movement of electrons during the interaction of donor-acceptor, which is influenced by ionization energy and electron affinity [85]. The maximum value of electrophilicity index is found for nano-cluster  $AgFeTe_2$  whereas the least value is observed for  $AuFeS_2$ .

The dipole moment of chalcopyrite-type nano-cluster  $XFeY_2$  is calculated in Debye. The result shows that minimum value of dipole moment is obtained for  $CuFeS_2$  whereas  $CuFeTe_2$  displays the maximum value. Nano-clusters  $CuFeTe_2$  and  $AgFeS_2$  display large dipole moment more than five Debye.

## Optical properties

In order to investigate the optical properties of chalcopyrite-type nano-clusters  $XFeY_2$ , we have calculated the optical electronegativity ( $\Delta\chi^*$ ), refractive index ( $n$ ), dielectric constant ( $\epsilon$ ) and IR and Raman activity. Pauling in his seminal work introduced the chemical bonding concept with the help of optical electronegativity [86]. According to Pauling's theory, optical electronegativity plays an important role in the ionicity. The computed optical electronegativity and refractive index of nano-cluster  $XFeY_2$  is presented in Figure 2. Refractive index of these clusters is obtained from Moss relation, Ravindra relation, Herve relation and Reddy relation. The result shows that the optical electronegativity and refractive index are interrelated with the energy gap of  $XFeY_2$ . Cluster with high energy gap displays the maximum value of optical electronegativity and the least value of refractive index. The maximum value of optical electronegativity (1.070 eV) is found for cluster  $AuFeS_2$ , whereas the minimum value (0.421 eV) is obtained for  $AuFeTe_2$ . The refractive index data obtained from Moss relation and Herve relation are close, whereas data computed from Reddy relation is higher. Computed data from these relationships clearly shows that nano-clusters  $CuFeTe_2$  and  $AuFeS_2$  display the maximum and minimum value of refractive index respectively. The result reveals that refractive index of  $XFeY_2$  increases from S to Se to Te. It follows similar order as reported previously for chalcopyrite-type semiconductors [57, 67, 74]. Refractive index of these chalcopyrite-type nano-clusters follow the trend as,  $n_{Cu-based} > n_{Ag-based} > n_{Au-based}$ .

Dielectric constant of chalcopyrite-type semiconductor material is intensely related with the refractive index. It is reported that refractive index of chalcopyrite-type materials is equal to square root of dielectric constant [60–62]. The computed dielectric constant of  $XFeY_2$  from Moss relation, Ravindra relation, Herve relation and Reddy relation are presented in Table 2. Computed data shows that dielectric constant of  $XFeY_2$  increases from S to Se to Te.

IR and Raman activity of chalcopyrite-type nano-clusters  $XFeY_2$  are reported in Figure 3. For  $CuFeS_2$  cluster, vibrational frequency is in the range of 0–406.55  $cm^{-1}$ . Maximum intensity of IR *i.e.* 36.433  $km/mol$  is

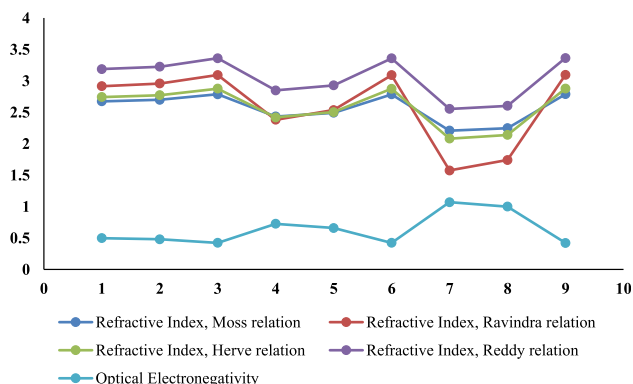


**Figure 2:** Optical electronegativity and refractive index of  $XFeY_2$  ( $X=Cu, Ag, Au$  and  $Y=S, Se, Te$ ) chalcopyrite-type nano-cluster.

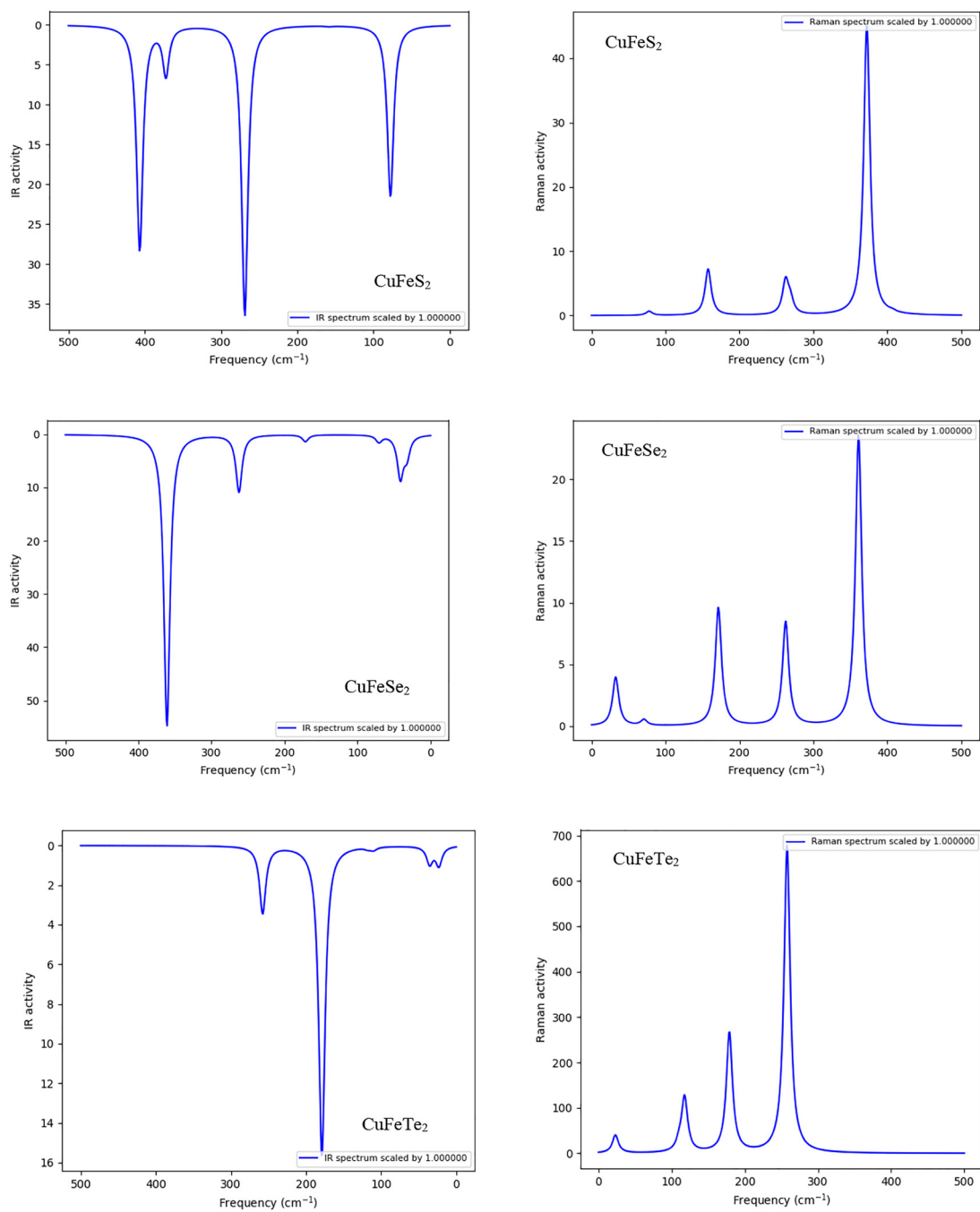


**Figure 3:** IR and Raman activity of  $XFeY_2$  ( $X=Cu, Ag, Au$  and  $Y=S, Se, Te$ ) chalcopyrite-type nano-cluster.

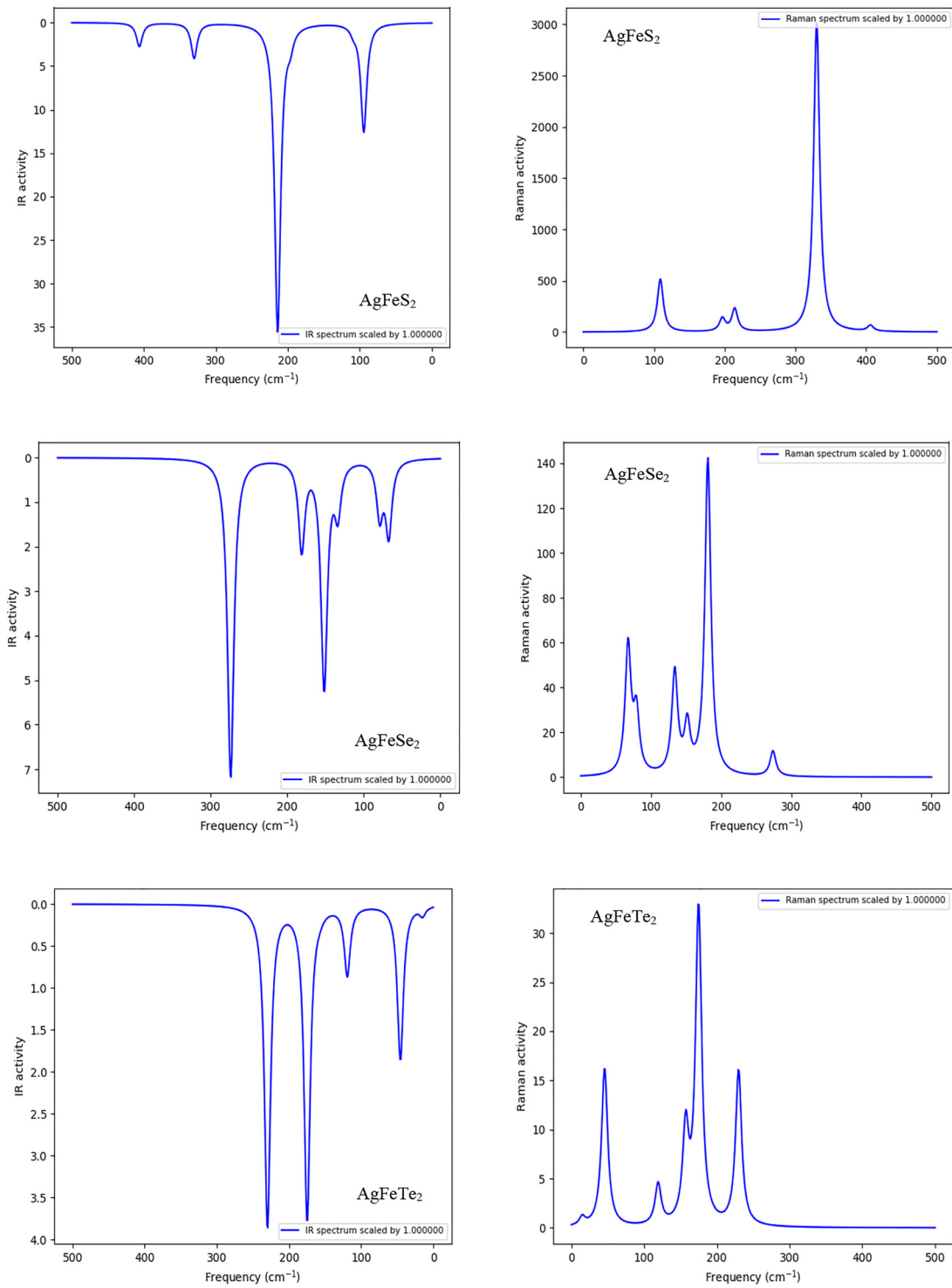


Figure 3: Continued.

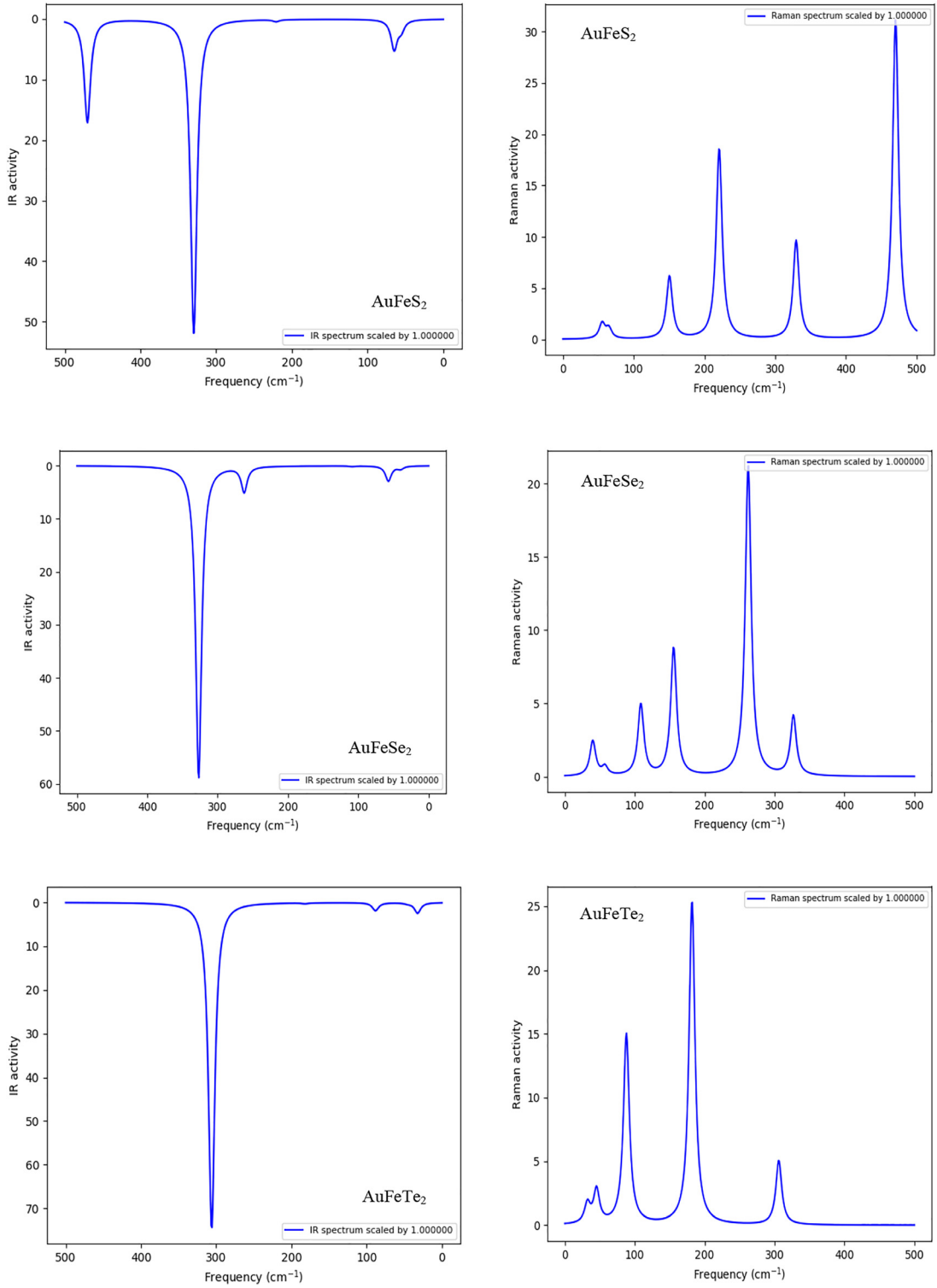


Figure 3: Continued.

**Table 2:** Dielectric constant of XFeY<sub>2</sub> (X=Cu, Ag, Au; Y=S, Se, Te) chalcopyrite-type nano-cluster.

Species	Moss relation	Ravindra relation	Herve relation	Reddy relation
CuFeS <sub>2</sub>	7.150	8.499	7.523	10.167
CuFeSe <sub>2</sub>	7.283	8.747	7.690	10.403
CuFeTe <sub>2</sub>	7.764	9.567	8.273	11.291
AgFeS <sub>2</sub>	5.923	5.670	5.854	8.116
AgFeSe <sub>2</sub>	6.213	6.432	6.265	8.580
AgFeTe <sub>2</sub>	7.757	9.555	8.264	11.277
AuFeS <sub>2</sub>	4.880	2.482	4.331	6.525
AuFeSe <sub>2</sub>	5.051	3.034	4.580	6.777
AuFeTe <sub>2</sub>	7.777	9.586	8.287	11.315

found at 268.73 cm<sup>-1</sup>. At the maximum frequency *i.e.* 406.55 cm<sup>-1</sup> intensity of IR is observed as 28.21 km/mol. The vibrational frequency is in the range of 0–360.96 cm<sup>-1</sup> for CuFeSe<sub>2</sub> cluster. Peak intensity of IR 54.81 km/mol is observed at 360.96 cm<sup>-1</sup>. For CuFeTe<sub>2</sub> cluster, vibrational frequency is in the range of 0–257.74 cm<sup>-1</sup>. Peak intensity of IR 15.75 km/mol is found at frequency 178.89 cm<sup>-1</sup>. At maximum frequency *i.e.* 257.74 cm<sup>-1</sup> intensity of IR is observed as 3.39 km/mol. For AgFeS<sub>2</sub>, vibrational frequency is observed in the range of 0–406.09 cm<sup>-1</sup>. Maximum intensity of IR *i.e.* 15.75 km/mol is found at 214.09 cm<sup>-1</sup>, whereas at maximum frequency 406.09 cm<sup>-1</sup> IR intensity is observed as 2.73 km/mol. Vibrational frequency for AgFeSe<sub>2</sub> cluster lies in the range of 0–273.91 cm<sup>-1</sup>. Peak intensity of IR *i.e.* 7.19 km/mol is observed at maximum frequency. Cluster AgFeTe<sub>2</sub> is having vibrational frequency in the range of 0–229.86 cm<sup>-1</sup>. IR intensity of 3.76 km/mol is found at 174.84 cm<sup>-1</sup>, whereas peak of IR intensity 3.84 km/mol lies at maximum frequency 229.86 cm<sup>-1</sup>. For AuFeS<sub>2</sub> vibrational frequency is in the range of 0–470.12 cm<sup>-1</sup>. Peak IR intensity 51.87 km/mol is found at 329.63 cm<sup>-1</sup>, however an intensity of 17.06 km/mol is observed at maximum frequency 470.12 cm<sup>-1</sup>. Vibrational frequency of AuFeSe<sub>2</sub> is found in the range of 0–326.94 cm<sup>-1</sup>. Maximum intensity of IR 59.02 km/mol is observed at maximum frequency, however weak intensity of 4.84 km/mol is found at 262.28 cm<sup>-1</sup>. For cluster AuFeTe<sub>2</sub> vibrational frequency is in the range of 0–306.03 cm<sup>-1</sup>. Maximum IR intensity 74.89 km/mol is observed at maximum frequency.

For cluster CuFeS<sub>2</sub>, three Raman spectra of magnitude 7.23, 5.15 and 45.39 a.u. are observed at frequency 157.65, 262.33 and 373.20 cm<sup>-1</sup> respectively. Raman spectra of less intensity 0.21 a.u. is also found at maximum frequency 406.55 cm<sup>-1</sup>. For CuFeSe<sub>2</sub> cluster, maximum intensity of Raman spectra 23.64 a.u. is found at frequency 360.96 cm<sup>-1</sup>. There are two other Raman spectra of magnitude 9.57 and 8.41 a.u. are found at frequency 171.45 and 262.37 cm<sup>-1</sup> respectively. The highest magnitude of Raman spectra 678.77 a.u. is found at frequency 257.73 cm<sup>-1</sup> for CuFeTe<sub>2</sub> cluster. At vibrational frequencies 117.61 and 178.89 cm<sup>-1</sup> Raman spectra of magnitude 121.50 and 265.61 a.u. are observed. For cluster AgFeS<sub>2</sub>, peak intensity of Raman 3029.65 a.u. is observed at 330.0 cm<sup>-1</sup>. Raman spectra of magnitude 517.82 a.u. is found at low frequency 108.86 cm<sup>-1</sup>, however at maximum frequency 406.09 cm<sup>-1</sup> Raman spectra of magnitude 57.87 a.u. is observed. For cluster AgFeSe<sub>2</sub>, highest magnitude of Raman spectra is found at frequency 181.14 cm<sup>-1</sup>. The second largest magnitude of Raman spectra 57.90 a.u. is observed at lowest vibrational frequency 67.40 cm<sup>-1</sup> whereas at maximum frequency 273.91 cm<sup>-1</sup> lowest magnitude of Raman spectra 11.33 a.u. is found. For AgFeTe<sub>2</sub> cluster, maximum magnitude of Raman spectra 32.34 a.u. is observed at 174.84 cm<sup>-1</sup>. Raman spectra of magnitude 15.87 a.u. is found at maximum frequency 229.86 cm<sup>-1</sup> whereas spectra 16.22 a.u. is observed at low frequency 45.60 cm<sup>-1</sup>. For cluster AuFeS<sub>2</sub>, the largest magnitude of Raman spectra 31.15 a.u. is observed at maximum frequency 470.12 cm<sup>-1</sup>. Raman spectra of less magnitude 6.12, 18.61 and 9.60 a.u. are found at frequencies 150.60, 220.86 and 329.63 cm<sup>-1</sup> respectively. For cluster AuFeSe<sub>2</sub>, highest magnitude of spectra 21.23 a.u. is found at 262.28 cm<sup>-1</sup>. Raman spectra of magnitude 4.90, 8.76 and 4.10 a.u., are observed at frequencies 108.72, 155.64 and 326.94 cm<sup>-1</sup> respectively. The largest magnitude of Raman spectra 25.46 a.u. is found at 181.89 cm<sup>-1</sup> for cluster AuFeTe<sub>2</sub>. At maximum frequency 306.03 cm<sup>-1</sup> Raman spectra of 5.04 a.u. is observed. The result reveals that vibrational frequency decreases from S to Se to Te.

For chalcopyrite-type nano-cluster CuFeS<sub>2</sub>, the computed bond lengths between d<sub>Cu-S</sub>, d<sub>Cu-Fe</sub> and d<sub>Fe-S</sub> are 2.296, 2.726 and 2.229 Å respectively. The computed bond lengths are in agreement with the experimental results. Hall and Stewart [87] reported experimentally the bond lengths between Cu-S and Fe-S are 2.302 and 2.257 Å respectively. Lazewski *et al.* [88] also reported bond lengths between Cu-S and Fe-S for CuFeS<sub>2</sub> by using DFT technique as 2.305 and 2.256 Å respectively. For cluster CuFeTe<sub>2</sub>, the bond lengths between d<sub>Cu-Fe</sub>, d<sub>Cu-Te</sub> and d<sub>Te-Te</sub> are calculated as 2.347, 2.618 and 2.812 Å respectively. Dzhabbarov *et al.* [89] reported the bond lengths between Cu-Fe for CuFeTe<sub>2</sub> as 2.5 Å. Bond length between Te-Te is reported by Abdullaev *et al.* [90] for CuFeTe<sub>2</sub> material as 2.6 Å.

## Conclusion

Structure, electronic and optical properties of iron-based chalcopyrite-type nano-cluster XFeY<sub>2</sub> are thoroughly investigated by using Density Functional Theory. The optimized ground state configurations and low-lying isomers of each cluster have real vibrational frequencies. The computed HOMO-LUMO energy gap is in the range of 1.568–3.982 eV, which specifies that these nano-clusters can be potential candidate for optoelectronic devices and solar cells. The data reveals that chalcopyrite-type material AuFeS<sub>2</sub> having star-shape geometry with point group C<sub>2v</sub> and spin multiplicity sextet displays the maximum stability with HOMO-LUMO energy gap of 3.982 eV. The result shows that HOMO-LUMO energy gap, optical electronegativity and vibrational frequency of XFeY<sub>2</sub> decreases from S to Se to Te, whereas refractive index and dielectric constant increases from S to Se to Te.

**Acknowledgement:** PR and TC are highly thankful to the Manipal University Jaipur, Jaipur and Sharda University, Greater Noida for their support to carry out the research. PKS would like to acknowledge the funding support from Science and Engineering Research Board (SERB) under Grant No. [EMR/2016/006259].

**Research funding:** This work was supported by Science and Engineering Research Board (SERB) under Grant No. [EMR/2016/006259].

## References

- [1] F. Hulliger. *Struct. Bond.* **4**, 83 (1968).
- [2] S. Conejeros, P. Alemany, M. Lluell, I. D. P. R. Moreira, V. Sanchez, J. Llanos. *Inorg. Chem.* **54**, 4840 (2015).
- [3] B. Sciacca, A. O. Yalcin, E. C. Garnett. *J. Am. Chem. Soc.* **137**, 4340 (2015).
- [4] L. P. Yu, R. S. Kokenyesi, D. A. Keszler, A. Zunger. *Adv. Energy Mater.* **3**, 43 (2013).
- [5] A. Chirila, P. Reinhard, F. Pianezzi, P. Bloesch, A. R. Uhl, C. Fella, L. Kranz, D. Keller, C. Gretener, H. Hagendorfer, D. Jaeger, R. Erni, S. Nishiwaki, S. Buecheler, A. N. Tiwari. *Nat. Mater.* **12**, 1107 (2013).
- [6] A. Chirila, S. Buecheler, F. Pianezzi, P. Bloesch, C. Gretener, A. R. Uhl, C. Fella, L. Kranz, J. Perrenoud, S. Seyrling, R. Verma, S. Nishiwaki, Y. E. Romanyuk, G. Bilger, A. N. Tiwari. *Nat. Mater.* **10**, 857 (2011).
- [7] C. Huang, Y. Chan, F. Y. Liu, D. Tang, J. Yang, Y. Q. Lai, J. Li, Y. X. Liu. *J. Mater. Chem. A* **1**, 5402 (2013).
- [8] D. S. Wang, W. Zheng, C. H. Hao, Q. Peng, Y. D. Li. *Chem. Commun.*, 2556 (2008). <https://doi.org/10.1039/B800726H>.
- [9] T. Omata, K. Nose, S. Otsuka-Yao-Matsuo. *J. Appl. Phys.* **105**, 73106 (2009).
- [10] C. Tablero. *Chem. Phys. Lett.* **499**, 75 (2010).
- [11] H. Bouhani-Benziane, O. Sahnoun, M. Driz, C. Daul. *J. Magn. Magn. Mater.* **396**, 345 (2015).
- [12] R. Merikhi, B. Bennecer, A. Hamidani. *J. Magn. Magn. Mater.* **424**, 327 (2017).
- [13] B. Djebour, H. Bouafia, B. Sahli, S. Hiadsi, B. Abidri. *J. Supercond. Nov. Magnetism* **31**, 1881 (2018).
- [14] L. I. Koroleva, D. M. Zashchirinskii, T. M. Khapaeva, A. I. Morozov, S. F. Marenkin, I. V. Fedorchenko, R. Szymczak. *J. Magn. Magn. Mater.* **323**, 2923 (2011).
- [15] G. B. Cha, W. S. Yun, S. C. Hong. *J. Magn. Magn. Mater.* **419**, 202 (2016).
- [16] N. Tsujii, T. Mori. *Appl. Phys. Express* **6**, 043001 (2013).
- [17] R. Ang, A. U. Khan, N. Tsujii, K. Takai, R. Nakamura, T. Mori. *Angew. Chem. Int. Ed.* **54**, 12909 (2015).
- [18] F. Ahmed, N. Tsujii, T. Mori. *J. Mater. Chem. A* **5**, 7545 (2017).

- [19] E. Dutkova, Z. Bujnakova, J. Kovaca, I. Skorvanek, M. J. Sayagues, A. Zorkovska, J. Kovac, Jr., P. Balaz. *Adv. Powder Technol.* **29**, 1820 (2018).
- [20] Y. H. A. Wang, N. Z. Bao, A. Gupta. *Solid State Sci.* **12**, 387 (2010).
- [21] X. Zheng, B. Sciacca, E. C. Garnett, L. Zhang. *ChemPlusChem* **81**, 1075 (2016).
- [22] H. Takaki, K. Kobayashi, M. Shimono, N. Kobayashi, K. Hirose, N. Tsujii, T. Mori. *Appl. Phys. Lett.* **110**, 072107 (2017).
- [23] M. Zhou, X. Gao, Y. Cheng, X. Chen, L. Cai. *Appl. Phys. A* **118**, 1145 (2015).
- [24] T. Djaafri, H. Bouafia, B. Sahli, B. Djebour, S. Ugur, G. Ugur, H. Moussa. *J. Magn. Magn. Mater.* **493**, 165730 (2020).
- [25] X. Peng, J. Liu, C. Ming, B. Li, Z. Zhao, K. Ye, M. Zeng, R. Zou, X. Lu, J. Hu. *Nanoscale* **12**, 11288 (2020).
- [26] K. Balasubramanian. *Relativistic Effects in Chemistry: Part A Theory and Techniques and Relativistic Effects in Chemistry*, John Wiley and Sons, New York (1997).
- [27] A. Berces. *J. Phys. Chem.* **100**, 16538 (1996).
- [28] P. Pyykko. *Chem. Rev.* **88**, 563 (1988).
- [29] T. Ziegler, J. G. Snijders, E. J. Baerends. *J. Chem. Phys.* **74**, 1271 (1981).
- [30] F. Boutaiba, A. Zaoui, M. Ferhat. *Superlattice. Microst.* **46**, 823 (2009).
- [31] K. Balasubramanian. *J. Phys. Chem.* **88**, 5759 (1984).
- [32] K. Balasubramanian, M. Han, M. Z. Liao. *J. Chem. Phys.* **86**, 4979 (1987).
- [33] K. Balasubramanian, C. Ravimohan. *J. Mol. Spectrosc.* **126**, 220 (1987).
- [34] P. Ranjan, S. Dhail, S. Venigalla, A. Kumar, L. Ledwani, T. Chakraborty. *Mater. Sci.* **33**, 719 (2016).
- [35] J. Hafner, C. Wolverton, G. Ceder. *MRS Bull.* **31**, 659 (2006).
- [36] P. Ranjan, T. Chakraborty. *Mater. Today Commun.* **22**, 100832 (2020).
- [37] P. Ranjan, T. Chakraborty. *J. Nanoparticle Res.* **22**, 35 (2020).
- [38] A. Poater, A. G. Saliner, R. Carbo-Dorca, J. Poater, M. Sola, L. Cavallo, A. P. Worth. *J. Comput. Chem.* **30**, 275 (2009).
- [39] M. Arockiaraj, J. Clement, K. Balasubramanian. *Polycycl. Aromat. Comp.* **40**, 280 (2017).
- [40] S. C. Basak, G. D. Grunwald, B. D. Gute, K. Balasubramanian, D. Opitz. *J. Chem. Inf. Comput. Sci.* **40**, 885 (2000).
- [41] K. Balasubramanian. *J. Math. Chem.* **55**, 195 (2017).
- [42] P. Bultinck, R. Ponc, R. Carbo-Dorca. *J. Comput. Chem.* **28**, 152 (2006).
- [43] R. Carbo-Dorca. *J. Comput. Chem.* **31**, 2452 (2010).
- [44] P. Bultinck, R. Carbo-Dorca. *J. Chem. Sci.* **117**, 425 (2005).
- [45] M. Sola. *Front. Chem.* **5**, 22 (2017).
- [46] J. Poater, M. Sola, C. Vinas, F. Teixidor. *Angew. Chem.* **53**, 12191 (2014).
- [47] M. J. Frisch, G. W. Trucks, H. B. Schlegel, G. E. Scuseria, M. A. Robb, J. R. Cheeseman, J. A. Montgomery, Jr., T. Vreven, K. N. Kudin, J. C. Burant, J. M. Millam, S. S. Iyengar, J. Tomasi, V. Barone, B. Mennucci, M. Cossi, G. Scalmani, N. Rega, G. A. Petersson, H. Nakatsuji, M. Hada, M. Ehara, K. Toyota, R. Fukuda, J. Hasegawa, M. Ishida, T. Nakajima, Y. Honda, O. Kitao, H. Nakai, M. Klene, X. Li, J. E. Knox, H. P. Hratchian, J. B. Cross, V. Bakken, C. Adamo, J. Jaramillo, R. Gomperts, R. E. Stratmann, O. Yazyev, A. J. Austin, R. Cammi, C. Pomelli, J. W. Ochterski, P. Y. Ayala, K. Morokuma, G. A. Voth, P. Salvador, J. J. Dannenberg, V. G. Zakrzewski, S. Dapprich, A. D. Daniels, M. C. Strain, O. Farkas, D. K. Malick, A. D. Rabuck, K. Raghavachari, J. B. Foresman, J. V. Ortiz, Q. Cui, A. G. Baboul, S. Clifford, J. Cioslowski, B. B. Stefanov, G. Liu, A. Liashenko, P. Piskorz, I. Komaromi, R. L. Martin, D. J. Fox, T. Keith, M. A. Al-Laham, C. Y. Peng, A. Nanayakkara, M. Challacombe, P. M. W. Gill, B. Johnson, W. Chen, M. W. Wong, C. Gonzalez, J. A. Pople. *Gaussian 03, Revision C.02*, Gaussian, Inc., Wallingford CT (2004).
- [48] H. Salehi, E. Gordanian. *Mater. Sci. Semicond. Process.* **47**, 51 (2016).
- [49] S. Ullah, H. U. Din, G. Murtaza, T. Ouahrani, R. Khenata, Naemullah, S. B. Omran. *J. Alloys Compd.* **617**, 575 (2014).
- [50] J. Liu, S. Chen, Q. Liu, Y. Zhu, Y. Lu. *Comput. Mater. Sci.* **91**, 159 (2014).
- [51] I. Aguilera, P. Palacios, P. Wahnnon. *Thin Solid Films* **516**, 7055 (2008).
- [52] B. Marsen, L. Steinkopf, A. Singh, H. Wilhelm, I. Laueremann, T. Unold, R. Scheer, H. W. Schock. *Sol. Energy Mater. Sol. Cells* **94**, 1730 (2010).
- [53] P. Palacios, K. Sanchez, J. C. Conesa, P. Wahnnon. *Phys. Status Solidi* **203**, 1395 (2006).
- [54] K. Hashikuni, K. Suekuni, H. Usui, R. Chetty, M. Ohta, K. Kuroki, T. Takabatake, K. Watanabe, M. Ohtaki. *Inorg. Chem.* **58**, 1425 (2019).
- [55] P. Ranjan, P. Kumar, T. Chakraborty, M. Sharma, S. Sharma. *Mater. Chem. Phys.* **241**, 122346 (2020).
- [56] R. G. Parr, W. Yang. *Density Functional Theory of Atoms and Molecules*, Oxford University Press, Oxford (1989).
- [57] R. R. Reddy, K. Ram Gopal, K. Narasimhulu, L. S. S. Reddy, K. R. Kumar, G. Balakrishnan, M. Ravi Kumar. *J. Alloys Compd.* **473**, 28 (2009).
- [58] J. A. Duffy. *Bonding, Energy Level and Bonding in Inorganic Solids*, Longman, England (1990).
- [59] J. A. Duffy. *J. Phys. C Solid State Phys.* **13**, 2979 (1980).
- [60] T. Moss. *Proc. Phys. Soc. B* **63**, 167 (1950).
- [61] T. Moss. *Photoconductivity in the Elements*, Academic Press Inc., New York (1952).
- [62] T. Moss. *Phys. Status Solidi B* **131**, 415 (1985).
- [63] N. M. Ravindra, S. Auluck, V. K. Srivastava. *Phys. Status Solidi B* **93**, K155 (1979).
- [64] V. P. Gupta, N. M. Ravindra. *Phys. Status Solidi B* **174**, K91 (1980).

- [65] P. J. L. Herve, L. K. J. Vandamme. *Infrared Phys.* **35**, 609 (1994).
- [66] P. J. L. Herve, L. K. J. Vandamme. *J. Appl. Phys.* **77**, 5476 (1995).
- [67] R. R. Reddy, K. Ram Gopal, K. Narasimhulu, L. S. S. Reddy, K. R. Kumar, C. V. K. Reddy, S. N. Ahmad. *Opt. Mater.* **31**, 209 (2008).
- [68] A. S. Verma, D. Sharma. *Phys. Scripta* **76**, 22 (2007).
- [69] D. C. Ghosh, S. Bhattacharyya. *Int. J. Mol. Sci.* **5**, 239 (2004).
- [70] B. Bhattacharyya, A. Pandey. *J. Am. Chem. Soc.* **138**, 10207 (2016).
- [71] S. K. Han, C. Gu, M. Gong, Z. M. Wang, S. H. Yu. *Small* **9**, 3765 (2013).
- [72] N. N. Kiselyova, V. A. Dudarev, M. A. Korzhuyev. *Inorg. Mater. Appl. Res.* **7**, 34 (2015).
- [73] B. Li, F. K. Yuan, G. J. He, X. Y. Han, X. Wang, J. B. Qin, Z. X. Guo, X. Lu, Q. Wang, I. P. Parkin, C. T. Wu. *Adv. Funct. Mater.* **27**, 1606218 (2017).
- [74] S. K. Tripathy. *Opt. Mater.* **46**, 240 (2015).
- [75] D. R. Lide. *Handbook of Chemistry and Physics*, CRC Press, USA (1999).
- [76] V. Kumar, A. Sinha, B. P. Singh, A. P. Sinha, V. Jha. *Chin. Phys. Lett.* **32**, 127701 (2015).
- [77] R. T. Sanderson. *Science* **114**, 670 (1951).
- [78] R. T. Sanderson. *Science* **116**, 41 (1952).
- [79] R. T. Sanderson. *Science* **121**, 207 (1955).
- [80] R. T. Sanderson. *J. Chem. Educ.* **29**, 539 (1952).
- [81] R. T. Sanderson. *Science* **31**, 238 (1954).
- [82] R. T. Sanderson. *Chemical Periodicity*, Reinhold Publishing Corporation, New York (1960).
- [83] R. G. Pearson. *J. Chem. Educ.* **64**, 562 (1987).
- [84] P. K. Chattaraj, S. Sengupta. *J. Phys. Chem.* **103**, 6122 (1999).
- [85] R. G. Parr, L. V. Szentpaly, S. Liu. *J. Am. Chem. Soc.* **121**, 1922 (1999).
- [86] L. Pauling. *The Nature of the Chemical Bond*, Oxford and IBH Pub. Co., Delhi (1969).
- [87] S. R. Hall, J. M. Stewart. *Acta Crystallogr. Sect. B Struct. Crystallogr. Cryst. Chem.* **B29**, 579 (1973).
- [88] J. Lazewski, H. Neumann, K. Parlinski. *Phys. Rev. B* **70**, 195206 (2004).
- [89] A. I. Dzhabbarov, S. K. Orudzhev, G. G. Guseinov, N. F. Gakhramanov. *Crystallogr. Rep.* **49**, 1136 (2004).
- [90] F. N. Abdullaev, T. G. Kerimova, G. D. Sultanov, N. A. Abdullaev. *Phys. Solid State* **48**, 1848 (2006).